The Journal of Chemical Physics

RESEARCH ARTICLE | MAY 12 2026

Structure and dynamics of confined water in naphthalene-diimide based molecular crystals

Special Collection: Festschrift in honor of Christoph Dellago: Exploring Paths and Barriers in Statistical Mechanics

Filippo Tommaso Garattoni ; Marco Severi ; Gabriele Amante; Christian B. Nielsen ; Giuseppe Cassone ; Daniele Fazzi

J. Chem. Phys. 164, 184509 (2026)
https://doi.org/10.1063/5.0318997

The Journal of Chemical Physics ARTICLE pubs.aip.org/aip/jcp

Structure and dynamics of confined water in naphthalene-diimide based molecular crystals

Cite as: J. Chem. Phys. 164, 184509 (2026); doi: 10.1063/5.0318997
Submitted: 22 December 2025 • Accepted: 11 April 2026 •
Published Online: 12 May 2026

Filippo Tommaso Garattoni,[1] Marco Severi,[1] Gabriele Amante,[2] Christian B. Nielsen,[3] Giuseppe Cassone,[2] and Daniele Fazzi[1,a)]

AFFILIATIONS

[1] Department of Chemistry "Giacomo Ciamician," University of Bologna, via Piero Gobetti 85, 40129 Bologna, Italy
[2] Institute for Chemical-Physical Processes, National Research Council of Italy, viale Ferdinando Stagno d'Alcontres 37, 98158 Messina, Italy
[3] Department of Chemistry, Queen Mary University of London, Mile End Road, London E1 4NS, United Kingdom

Note: This paper is part of the Special Topic Festschrift in Honor of Christoph Dellago: Exploring Paths and Barriers in Statistical Mechanics.
[a)] **Author to whom correspondence should be addressed:** daniele.fazzi@unibo.it

ABSTRACT

Under confinement, water changes its structure and dynamics, displaying new properties with respect to the bulk. We studied water confined in naphthalene diimide (NDI)-based molecular crystals via classical molecular dynamics simulations. We examined NDIs functionalized with either hydrophilic linear triethylene glycol side chains (NDI-TEG) or hydrophobic *n*-hexyl chains (NDI-C6), increasing the hydration (i.e., amount of water molecules within each crystal) up to a 1:3 NDI:water molar ratio. Static and dynamical properties of confined water are compared to those of room-temperature and supercooled (200 K) bulk water, which serve as references for liquid and glassy states, respectively. The impact of confinement is analyzed through structural order parameters, time-dependent correlation functions, and hydrogen-bond (HB) analyses. At low hydration (≈1:1 NDI:water), confined water assumes a structural order that is far from the tetrahedral one, showing different spatial organizations when inserted within hydrophilic NDI-TEG or hydrophobic NDI-C6 crystals. By increasing the hydration level (≈1:3 NDI:water), the structure of confined water clusters shifts toward a more bulk-like (liquid) arrangement, while the chemical nature of the NDI side chains plays a marginal role. Notably, fast (sub-*ps*) and slow (hundreds of *ns*) water dynamics are not much influenced by the hydrophilicity/hydrophobicity of the side chains but rather by confinement effects. The analysis of the HB network autocorrelation functions highlights how finite-size effects and restricted connectivity are the main factors controlling HB dynamics. Our study paves the way toward an atomistic understanding of both structural and dynamical functions of water confined in molecular crystals, opening new paths for the rationalization of transport phenomena in the emerging class of organic mixed ionic-electronic conductors.

INTRODUCTION

The structural and dynamical properties of confined water differ dramatically from those of the bulk phase,[1–3] resulting in altered hydrogen-bond (HB) networks[4–6] and reactivity,[7–10] modified diffusion mechanisms,[11,12] and different dielectric responses.[13–16] Such effects play a prominent role in governing proton and ion transport,[17–20] redox stability,[21,22] and electrochemical capacitance.[23] Water under confinement is ubiquitous in nature, as the case of protein-binding pockets, membrane-protein channels, membrane pores,[24,25] and nonbiological macromolecules as polymer-based microgels.[26,27] At the same time, it is possible to artificially confine water in various low-dimensional materials, such as in nanotubes,[28,29] graphene layers,[30] molecular crystals,[31] and metal-organic frameworks,[32,33] thus enabling the usage of nanoconfined water in opto-electronic, energy storage, and conversion applications. Understanding how water changes its short- and long-range structure, as well as its fast- and slow-time dynamics, is therefore

instrumental to the rational design of new complex systems for bio-interfacing[34] and energy-saving devices.[35,36]

Here, we explore the collective behavior of water molecules when confined in organic functional materials, such as naphthalenediimide (NDI) based molecular crystals. NDIs are soft conjugated materials studied as organic semiconductors[37] and, recently, as organic mixed ionic-electronic conductors (OMIECs).[38] OMIECs are an emerging class of functional materials, finding potential applications in bioelectronics,[36] energy-saving technologies (e.g., batteries and supercapacitors)[39] and electrochemical transistors.[40] OMIECs are an ideal platform to translate chemical signals into electrical signals (and vice versa), thus being able to emulate synaptic weights in artificial neural networks.[36] OMIECs can conduct both ionic and electronic charges (e.g., electron and hole),[36,41] where ion transport is generally promoted by the contact with an aqueous solution [e.g., 0.1M NaCl (aq)].[42] The way water molecules are absorbed and self-organized within the bulk of molecular materials is a fine balance between intermolecular hydrophilic and hydrophobic interactions occurring in a low-dimensional environment. Such a delicate equilibrium governs the static and dynamical properties of confined water and ultimately impacts the structural and transport (e.g., ion diffusion) functionalities of OMIECs. While in literature there is a consistent body of work on the effect of hydration on OMIECs' structure (e.g., film swelling),[43–48] the atomistic description of water properties upon low-dimensional confinement in OMIECs remains largely unexplored.

Recently, Siemons *et al.* reported a qualitative perspective on the importance of OMIEC–water interactions.[48] They reviewed the latest contributions documenting how water's presence influences swelling, ion solvation, dielectric properties, and redox potentials in polymer based OMIECs. Despite numerous experimental investigations, atomistic studies assessing the structure and dynamics of water molecules confined in OMIECs' bulk are very limited. For instance, Nelson *et al.* investigated via extensive molecular dynamics (MD) and metadynamics simulations the penetration of water molecules into alkoxylated and glycolated polythiophene OMIECs.[42,45,49] Their studies were pivotal for revealing the importance of balancing hydrophilic and hydrophobic side chains to control both water penetration (e.g., polymer swelling) and electrochemical properties of OMIECs. Wang *et al.*, instead, reported an elegant experimental and computational investigation studying water-mediated ion transport in an anion-organic polymer-based exchange membrane. They revealed how the local structure of water governs the ion transport, showing that faster ion diffusion occurs only when a robust hydrogen network is formed.[50]

Despite these fundamental findings, in-depth atomistic studies focusing on the structure and dynamics of water molecules when confined in OMIEC molecular crystals are missing. We believe that modeling and characterizing the role of confined water in OMIECs would be beneficial for understanding the mixed transport properties (e.g., both charge and mass diffusion), as well as for drafting structure–function relationships useful to guide materials design.

Here, by adopting classical force-field MD simulations, we investigate the spatial and time-dependent properties of water when confined in bulk **NDI** molecular crystals, namely, hydrophilic **NDI-TEG**,[51] which bears linear triethylene glycol side chains, and hydrophobic **NDI-C6**[52–54] functionalized with *n*-hexyl side chains (Fig. 1).

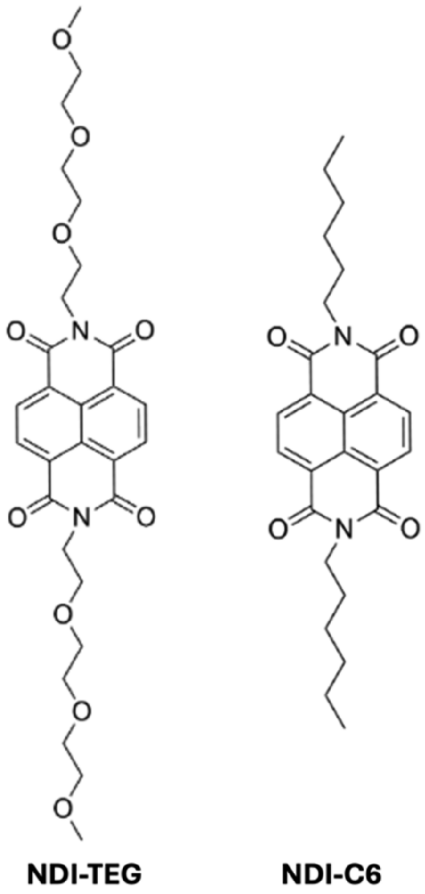

FIG. 1. Chemical structures of **NDI-TEG** (left) and **NDI-C6** (right).

Different amounts of water molecules are inserted into the bulk of **NDI** crystals to study the effects of confined water as a function of crystal hydration and with respect to the different hydrophilicity of the side chains (**TEG** vs **C6**). As a reference to interpret our results, we performed MD simulations of both bulk water under ambient conditions and in a supercooled regime (i.e., 200 K), the latter representing a commonly employed benchmark in the literature to compare with confined (nanometer scale) water environments.[55,56]

In this paper, we employed the tetrahedral order parameter[57] and the Lechner–Dellago bond orientational order parameters[58] to investigate the static structural properties, while we resort to time-dependent autocorrelation functions to characterize the structural, translational, rotational, and HB network dynamics. We discuss the subtle interplay between confinement effects and chemical interactions between water molecules and **NDI** side chains, underlying the overall behavior of water within the **NDI** molecular crystals. While the hydrophilicity/hydrophobicity of the side chains plays a role in affecting the water structural properties at low hydration levels (e.g., 1:1, NDI:water), for higher ratios (e.g., 1:3), both water structure and dynamics are not much influenced by the nature of the side chains, rather by confinement effects. Our analysis is instrumental

for understanding the structure and dynamics of water when inserted into the bulk of functional molecular materials and, ultimately, to design OMIECs with optimal transport properties in aqueous and biocompatible solutions.

METHODS

Molecular dynamics

Molecular dynamics (MD) simulations were performed via LAMMPS-2Aug2023[59] on a 4 × 4 × 6 **NDI-TEG** supercell and on a 5 × 5 × 4 **NDI-C6** supercell, corresponding to 96 NDI molecules in each simulation box. The force field employed is taken from our previous work on NDIs,[51] where we studied via MD simulations the bulk single crystal structure of **NDI-C10** (n-decyl side chains) and **NDI-TEG**, as well as the amorphous structure of **NDI-crown** (glycol based 15-crown-5 rings). The bonded parameters were mutated from the OPLS-AA force field,[60] and the non-bonded parameters were computed *ex-novo* following the Tkatchenko–Scheffler (T–S) approach.[61–63] The partial charges were derived by employing the DDEC6 (density-derived electrostatic and chemical electron density partitioning) scheme.[64–67] DDEC6 charges were computed using the Chargemol program. Water molecules were described with the OPC3 force field,[68] which is able to reproduce the structural and dynamical properties of bulk water at room temperature, such as the dielectric constant, the self-diffusion coefficient, and the coordination number of the first solvation shell.[69] Then, the same simulation protocol has been employed for the **NDI-TEG** and **NDI-C6** supercells. After an initial equilibration of the pristine material (i.e., molecular crystals without inclusion of water molecules, see the supplementary material for details), water insertion was performed in the NPT ensemble at 300 K and 1 atm by randomly placing a single water molecule in the simulation cell every 100 ps. We selected three cases corresponding to the inclusion of 100, 200, and 300 water molecules in the simulation box, representing roughly the cases of 1:1, 1:2, and 1:3 NDI:water ratio. Such hydration levels do not significantly alter the **NDI** crystal structures, preserving the molecular packing. This is confirmed by the computed nitrogen–nitrogen radial distribution functions for the NDI:water ratio (e.g., 1:3) as compared to the pristine single crystal case (see Fig. S4 in the supplementary material). However, further preliminary calculations, which would deserve future in-depth studies, showed that the inclusion of a higher amount of water (e.g., 500 H_2O, ~1:5 ratio) resulted in huge alterations of the bulk structure (i.e., molecular packing) for **NDI-TEG**, with the formation of large water clusters and the break of the π–π interactions between **NDI** planes. For **NDI-C6**, instead, the molecular packing seems to be preserved, and NDIs rearrange as a whole (collective swelling) to accommodate large water clusters. Preliminary structures for the 1:5 ratios are reported in Fig. S6 of the supplementary material; however, they will not be discussed in-depth in the current study. For each hydration level, a production run (NPT ensemble) at 300 K and 1 atm was performed for 200 ns. For the calculation of the mean square displacements, the trajectories were lengthened up to 500 ns. MD simulations of pristine water (i.e., bulk water) were performed by considering two boxes contaning 3000 molecules each at temperature of 300 K and 200 K, respectively. The computational workflow applied was the same as reported above for the **NDI** systems.

Structural and dynamical analyses

For the analysis of the local structure and spatial correlations of water molecules in condensed phases, we draw inspiration from the extended literature on order parameters.[70–72] We selected two such parameters to characterize the local structure of water: the tetrahedral orientational order parameter (q) and the Lechner–Dellago bond orientational order parameters (q_l). We employ the tetrahedral order parameter as proposed by Errington and Debenedetti,[57]

$$q = 1 - \frac{3}{8}\sum_{j=1}^{3}\sum_{k=j+1}^{4}\left(\cos\psi_{jk} + \frac{1}{3}\right)^2, \tag{1}$$

where ψ_{jk} is the angle formed by the lines joining the oxygen atom of a water molecule and its nearest neighbor oxygen atoms j and k. For a perfect tetrahedral arrangement (e.g., ice I_h), it attains a value of 1, while for an ideal gas with randomly distributed particles, the mean value vanishes. It is worth noticing that q can assume negative values: for example, a 1D linear chain of water molecules is characterized by a tetrahedral order parameter $q = -1$. Notably, the tetrahedral orientational order parameter does not consider the mutual distance between water molecules, but only their angular distribution.

We also employ the Lechner–Dellago order parameters,[58,73] extensively used in the description of local structural order in amorphous systems[74] and in the identification of ordered structures, e.g., crystals, showing different spatial groups.[71] Given a molecule i with its nearest neighbor j, the r_{ij} vector connecting molecules i and j can be expressed in spherical coordinates $\theta(r_{ij}), \phi(r_{ij})$. In this frame of reference, it is possible to define a spherical harmonic function $Y_l^m(\theta,\phi)$. By considering the total number of first nearest neighbors of molecule i, $N_b(i)$, Steinhardt proposed[73] an averaged bond orientational order parameter defined as

$$q_{lm}(i) = \frac{1}{N_b(i)}\sum_{j=1}^{N_b(i)} Y_l^m(\theta,\phi), \tag{2}$$

where l and m are the degree and order of the spherical harmonic, respectively. Starting from Eq. (2), another set of bond orientational order parameters was introduced by Lechner and Dellago to better discriminate different local environments (e.g., amorphous materials) and crystal structures.[58,75] The modification consisted of introducing a further averaged form of $q_{lm}(i)$ to include also the second shell as

$$\langle q_{lm}\rangle(i) = \frac{1}{N_b(i)+1}\sum_{j=1}^{N_b(i)+1} q_{lm}(j). \tag{3}$$

The order parameter in Eq. (3) can be averaged over the order of the spherical harmonics, obtaining rotationally invariant combinations as

$$\langle q_l\rangle(i) = \sqrt{\frac{4\pi}{2l+1}\sum_{m=-l}^{l}|\langle q_{lm}\rangle(i)|^2}. \tag{4}$$

In this work, we will report the values of $\langle q_l\rangle$, respectively, as reported in Eq. (4). Both q and $\langle q_l\rangle$ were calculated with an in-house developed Python program. We complemented the structural analysis by computing the oxygen radial distribution function (RDF) of water molecules, performed with TRAVIS.[76,77]

The dynamics of water molecules was analyzed by computing both the mean square displacement (MSD) of the oxygen coordinates (as suggested in Refs. 76 and 77) and employing various types of autocorrelation functions. The first computed autocorrelation function concerns the tetrahedral order parameter q, which reads as[78]

$$C_q(t) = \frac{\langle q(t)q(0)\rangle - \langle q(0)\rangle^2}{\langle q(0)^2\rangle - \langle q(0)\rangle^2}. \quad (5)$$

The decay of $C_q(t)$, calculated for a single molecule, represents the time needed to witness a complete rearrangement of the initial ($t = 0$) configuration. We emphasize that the decay of $C_q(t)$ can be calculated for different initial configurations, irrespective of the value of the order parameter q. A complete decay of $C_q(t)$ means that the first four neighbors of a water molecule have been rearranged to a different conformation. In-house python based-codes (available upon request) have been used for the calculation of the tetrahedral [Eq. (1)] and bond orientational order parameteres [Eq. (4)], as well as for the autocorrelation function $C_q(t)$ [Eq. (5)]. Another useful autocorrelation function to study the dynamics of water is the reorientational time-correlation function (TCF), defined as

$$C_2(t) = \langle P_2[u(0)\cdot u(t)]\rangle, \quad (6)$$

where $u(t)$ is the vector connecting an oxygen atom of water to one of its bound hydrogen atoms at time t and P_2 is the second-order Legendre polynomial.[79] $C_2(t)$ is a measure of how long the OH bond vector remains aligned with itself over time, that is, how long water molecules maintain their initial orientation.

Hydrogen Bond (HB) analysis

To quantify the HB network dynamics, the HB autocorrelation functions employing the Luzar–Chandler geometrical definition[80] were computed. Within this framework, a HB between a donor (D) and an acceptor (A) water molecule is identified whenever both conditions are satisfied: (i) the intermolecular distance between oxygen atoms is shorter than a threshold ($r^c_{OO} < 3.5$ Å) and (ii) the angle $\angle O_D - H - O_A$ is smaller than a cutoff ($\theta^c < 30°$). Under these constraints, we define a binary function $h_{i,j}(t)$, which equals 1 if a specific D–H···A pair (i, j) is hydrogen-bonded at time t, and 0 otherwise.

We evaluated two autocorrelation functions, here denoted as *continuous* and *persistent*. The *continuous* correlation quantifies the probability that a given bond present at time *0* survives uninterrupted up to time t. It therefore decays at the first breaking event and provides an estimate of the intrinsic lifetime of a single, *continuously* intact HB. To this aim, a function $H_{i,j}(t)$ is introduced, assuming a value of 1 only if the original bond remains *continuously* intact from time 0 to t, so that the *continuous* autocorrelation reads as

$$C_C(t) = \frac{\langle h_{i,j}(0)H_{i,j}(t)\rangle}{\langle h_{i,j}(0)\rangle}. \quad (7)$$

The *persistent* autocorrelation function measures the probability that a given bond present at time 0 is again present between the same donor–acceptor pair (i, j) after a delay t, irrespective of what happens in between (the bond may break and reform multiple times during the interval [0–t]). It is defined as

$$C_P(t) = \frac{\langle h_{i,j}(0)h_{i,j}(t)\rangle}{\langle h_{i,j}(0)\rangle}. \quad (8)$$

Because it only checks the bond state at the beginning and at the end of the time interval, $C_P(t)$ is primarily sensitive to long-time network reorganization and partner exchange processes. This implies that, contrary to the *continuous* autocorrelation function that can only either keep constant or decrease in time, the *persistent* one could, in principle, also have a non-monotonic behavior, climbing back up in value. Furthermore, we note passing that the *persistent* autocorrelation function should not be confused with the *intermittent* one also used in the literature. To avoid state-dependent (biased) values, 50 000 windows were sampled by starting from randomly selected frames, hence varying the 0 time start. The in-house C++ code for the calculation of Eqs. (7) and (8) is available upon request.

RESULTS AND DISCUSSION

Inspection of the simulation boxes for both **NDI-TEG** and **NDI-C6** after 200 ns of MD simulation confirmed that both crystal structures are overall preserved in the presence of various water contents, namely, in the NDI:water ratios ranging from 1:1 up to 1:3. Water insertion causes local distortions (see Fig. 2); however, the overall molecular packing and side chain arrangements are maintained. In the case of 100 water molecules (1:1 ratio), we observe that in **NDI-C6** [Fig. 2(a)], water self-organizes in small clusters, mainly localized within the free volume between the columnar stacks of NDI molecules. For **NDI-TEG** [Fig. 2(b)], the water clusters are more uniformly distributed throughout the crystal, lying on average along with the TEG chains. As displayed in Fig. 2(c), increasing the NDI:water ratio up to 1:3 (300 water molecules) causes the water clusters in **NDI-C6** to grow, expanding among the free volume between the alkyl chains, however, without disrupting the NDI π–π staking. For **NDI-TEG**, fewer but larger clusters than **NDI-C6** are formed (see cluster analysis in the supplementary material), also preserving the NDI packing motif for this case, as shown in Fig. 2(d).

Going beyond the qualitative visual inspection toward a quantitative structural characterization of the confined water clusters, we compute the orientational tetrahedral [q, Eq (1)] and the Lechner–Dellago local bond orientational order parameters [q_4, q_6, Eq (4)]. We only report the results for the systems containing 100 and 300 water molecules, since the case with 200 water molecules shows intermediate behavior between the two, as reported in the supplementary material.

In Figs. 3(a)–3(c) the distributions of q [$P(q)$] are reported, while the Lechner–Dellago bond orientational order parameters, in the $\langle q_4\rangle - \langle q_6\rangle$ plane, are displayed in Figs. 3(b)–3(d). The cases of confined water in **NDI-TEG** and **NDI-C6** crystals in different ratios [1:1—upper panels (a) and (b) and 1:3—bottom panels (c) and (d)], are compared with the cases of bulk (liquid) water at room temperature (300 K, black) and supercooled (200 K, gray).

$P(q)$ for bulk water at 300 K is in agreement with that reported by Errington and Debenedetti.[57] The tetrahedral parameter shows a

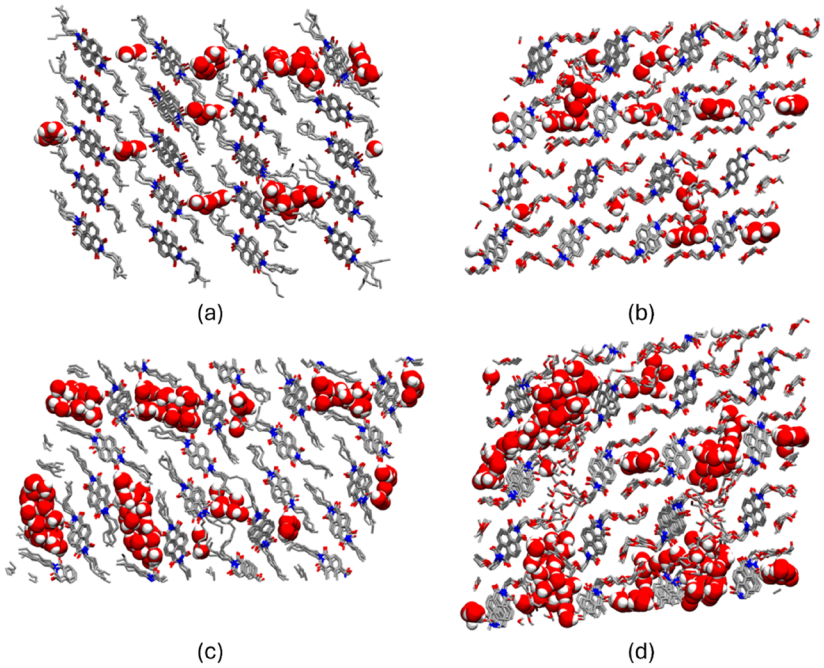

FIG. 2. Simulation boxes (a 4 × 4 × 6 **NDI-TEG** supercell and on a 5 × 5 × 4 **NDI-C6** supercell) after a 200 ns simulation. Panel (a): **NDI-C6** and 100 water molecules (1:1). Panel (b): **NDI-TEG** and 100 water molecules (1:1). Panel (c): **NDI-C6** and 300 water molecules (1:3). Panel (d): **NDI-TEG** and 300 water molecules (1:3).

bimodal distribution, indicating the existence of two distinct populations of local arrangements, where either a molecule and its four nearest neighbors exhibit the tendency to be structured in an *ice-like* manner ($q > 0.6$), or the environment around a given molecule is less structured ($q < 0.6$). In supercooled conditions, i.e., 200 K, the $P(q)$ distribution gets narrower and shifts toward higher q values, mirroring the expected increase in the orientational order toward more tetrahedral local structures. In contrast, the computed $P(q)$ of confined water into **NDI-TEG** and **NDI-C6** crystals dramatically departs from those of the bulk. As shown in Fig. 3(a) for the 1:1 NDI:water ratio [100 water molecules, Figs. 3(a) and 3(b)], $P(q)$ associated with the **NDI-C6** crystal is very broad, with a plateau centered around zero, reflecting an overall lack of tetrahedral order for confined water. Despite that, confinement allows for the exploration of local linear topologies as testified by the non-negligible sampling of negative q values close to, and even smaller than, −1. In **NDI-TEG**, $P(q)$ is narrower than in **NDI-C6**, and it is centered on negative values ($q \sim -0.4$). Considering that q equals −1 for a linear chain of four molecules, a distribution peaked on negative values suggests that water molecules are *prevalently* confined in a columnar fashion within this NDI crystal. Indeed, water clusters confined in **NDI-TEG** adopt an *elongated* shape throughout the whole crystal thickness. For low water contents (e.g., 100 molecules, 1:1 ratio), the presence of hydrophilic triethylene glycol side-chains (-TEG) induces a more prominent local structural ordering of water clusters, resembling column-like aggregates, while hydrophobic lateral chains (-C6) promote less structured (or disordered) nano-clusters, as reflected by a broader distribution.

By increasing the water content, up to 300 molecules (1:3 ratio), the effect of the side-chain chemistry (i.e., hydrophilicity/hydrophobicity characters) on the tetrahedral order parameter is negligible. As shown in Fig. 3(c), the distributions computed for water confined in **NDI-TEG** and **NDI-C6** are similar, and they both shift toward more positive q values ($q \sim 0.3$–0.5). Such shifts suggest an increased tetrahedrality and a decreased linearity of confined water than the previous low-content cases (i.e., 1:1 ratio). For water confined in **NDI-C6**, $P(q)$ is peaked to higher values than **NDI-TEG**, possibly indicating a slightly but measurable higher tetrahedral order.

To further elucidate the local structure of confined water, we employed the Lechner–Dellago bond orientational order parameters, specifically $\langle q_4 \rangle$ and $\langle q_6 \rangle$, which are commonly used to characterize the local environment of a particle.[58,75] Given their functional form (i.e., spherical harmonics), $\langle q_4 \rangle$ and $\langle q_6 \rangle$ allow for characterizing local symmetries and environments beyond the tetrahedral arrangement. As reported in Figs. 3(b)–3(d), analyses of bulk water at 300 and 200 K show that the centroids of the $\langle q_4 \rangle / \langle q_6 \rangle$ are close to each other, with supercooled water showing slightly higher values than its room-temperature counterpart, reflecting an overall similar local bond orientational structure. Nevertheless, for the supercooled regime, we observe that the limited phase space exploration leads to a reduced distribution of the $\langle q_4 \rangle / \langle q_6 \rangle$ Lechner–Dellago bond orientational order parameters than the 300K liquid case. Moving to the cases of confined water in NDI crystals, for 100 water molecules [Fig. 3(b)], the $\langle q_4 \rangle / \langle q_6 \rangle$ scatterplot appears very sparse, and the centroids shift to higher values compared to bulk water. The observed shift indicates a higher degree of local bond orientational order, even though very large deviations from the centroid behavior witness a multifaceted set of local environments. Interestingly, the $\langle q_4 \rangle / \langle q_6 \rangle$ distribution presents the same centroid for both **NDI-TEG** and **-C6**, therefore not revealing specific differences in the local structure, conversely to the tetrahedral order parameter q. By increasing the content of water up to 300 molecules [Fig. 3(d)], the $\langle q_4 \rangle / \langle q_6 \rangle$ distribution centroid moves to lower values toward the bulk cases. A tiny difference between **NDI-TEG** and **NDI-C6** emerges, though.

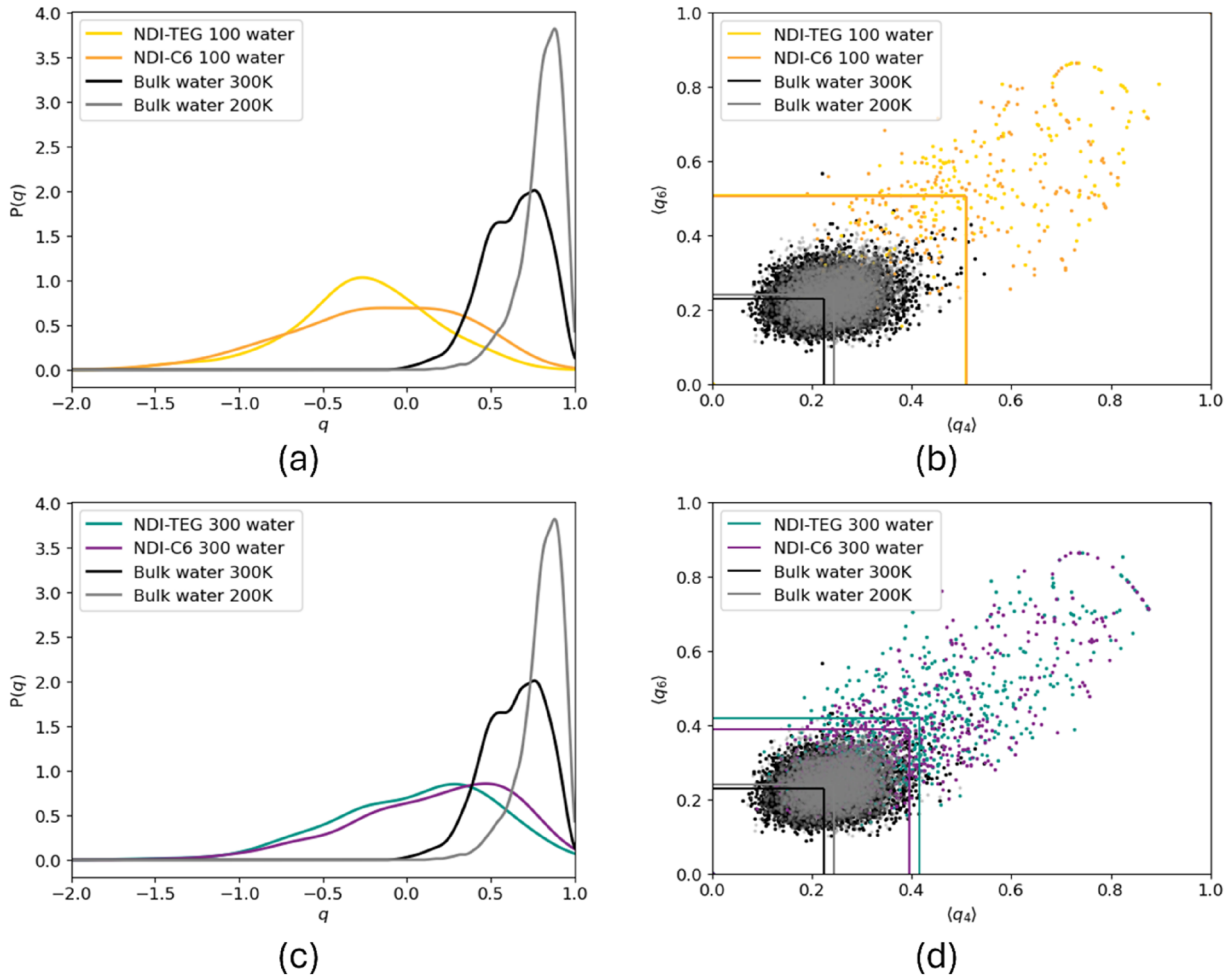

FIG. 3. Water structural analyses in **NDI-TEG** and **NDI-C6** crystals. Panels (a)–(c): Tetrahedral order parameter distribution $P(q)$ for the cases of 100 and 300 inserted water molecules. Panels (b)–(d): Lechner–Dellago bond orientational order parameters in the $\langle q_4 \rangle - \langle q_6 \rangle$ plane for 100 and 300 water molecules (solid lines represent the centroid of the distributions). In all panels, the black solid line refers to bulk water at 300 K, and gray lines correspond to supercooled bulk water at 200 K.

Confined water in **NDI-C6** assumes a local bond orientational structure closer to bulk water than water confined in **NDI-TEG**, paralleling the trends observed for the tetrahedral order parameter [Fig. 3(c)].

These structural insights hint at the fact that the hydrophilicity and hydrophobicity characters of the lateral chains play an active role in shaping the water nano-clusters at low water contents (e.g., 1:1 NDI:water ratio), while such effects become negligible when the water content increases (e.g., up to 1:3). In the latter case, the hydrogen-bond interactions within the water aggregates dominate, driving the confined clusters toward bulk-like properties.

To further test this assumption, we next examine the time-dependent (dynamical) behavior of water under confinement in NDI molecular crystals. To do so, we consider a variety of time-dependent properties, namely, the mean square displacement (MSD) of the water oxygens, the time-dependent autocorrelation function of the local tetrahedral order $C_q(t)$ [Eq. (5)], the reorientational motions via the $C_2(t)$ auto-correlation function [Eq. (6)], and the hydrogen bond network analysis via the $C_C(t)$ and $C_p(t)$ autocorrelation functions [Eqs. (7) and (8)].

Figures 4(a)–4(c) show the log–log plot of the MSD of water molecules computed over 30 ns (see Refs. 76 and 77) for 1:1 and 1:3 NDI:water ratios, respectively, averaging over a 100 ns MD trajectory after 400 ns of equilibration. While for bulk water at room temperature, the MD simulations are sufficiently long to reach a diffusive regime (MSD ~ t); for the cases of supercooled water (200 K) and confined water in NDI crystals, the regime is still non-diffusive (MSD ~ t^{α}, with $0.94 \leq \alpha \leq 1.08$). At 300 K, bulk water exhibits the largest MSD values, as expected for a liquid phase. At 200 K, the translational motion is significantly hindered, resulting in an MSD two or three orders of magnitude lower than at room temperature and hence reflecting the (slow) transition toward a glassy-like state. Under confinement into the NDI molecular crystals, water mobility is markedly reduced as compared to the room temperature bulk phase, with MSD values one or two orders of magnitude lower. For 1:1 NDI:water (100 water molecules), the MSD of confined

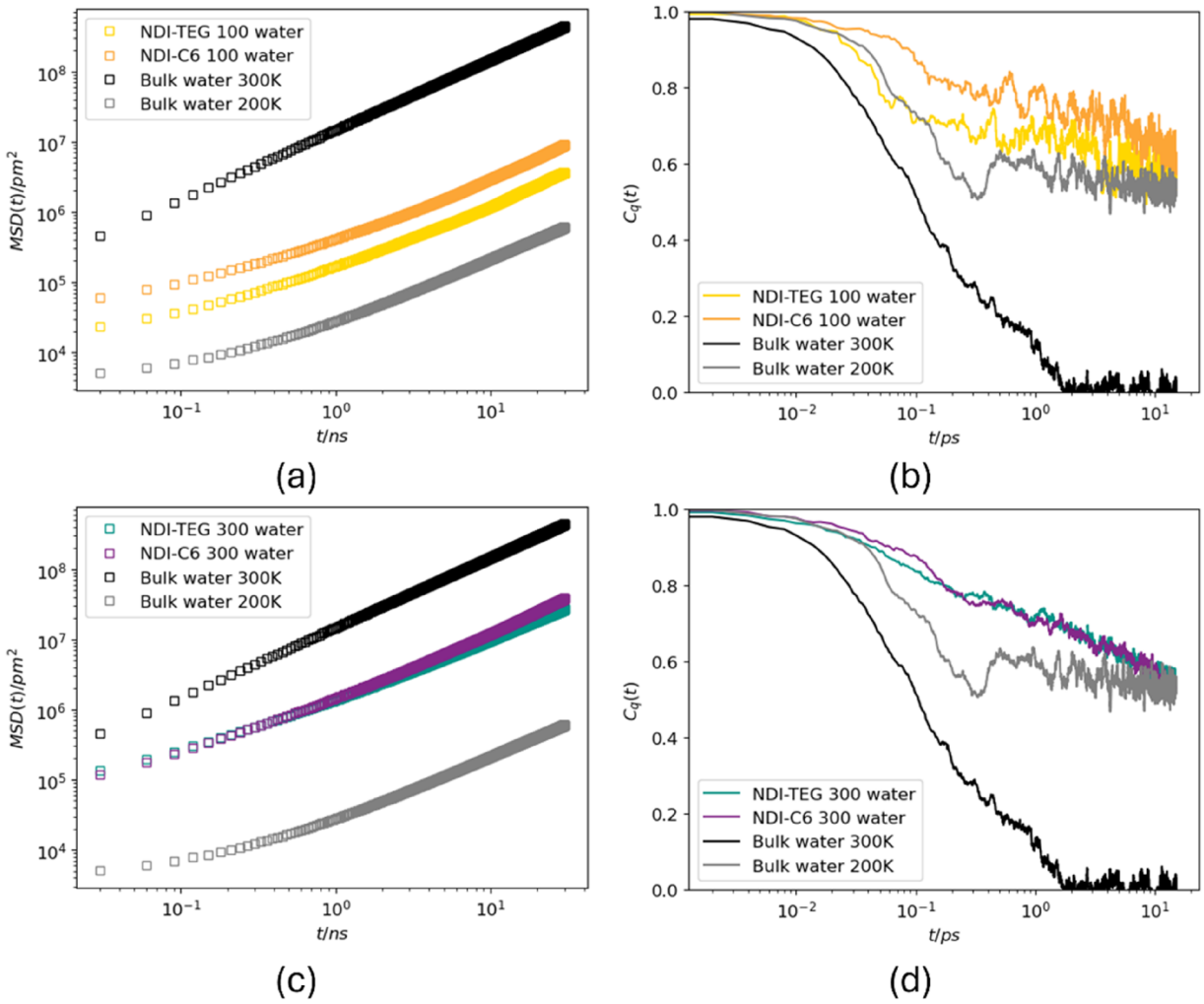

FIG. 4. Mean square displacement (MSD) computed for 100 (panel a) and 300 water molecules (panel c) confined in **NDI-TEG** and **NDI-C6**. Autocorrelation function [$C_q(t)$] of the tetrahedral order parameter q for the case of 100 (panel b) and 300 water molecules (panel d) confined in **NDI-TEG** and **NDI-C6**. In each panel, data referring to bulk water at 300 K are reported in black, while in supercooled conditions (200 K), data are reported in gray.

water is closer to that of supercooled bulk water than that of room-temperature conditions, indicative of an intermediate situation between a glass-like and a liquid-like behavior. With respect to the hydrophilicity and hydrophobicity of the lateral chains, the presence of hydrophobic pendants, as in **NDI-C6**, better favors the translational displacements of nanoconfined water than **NDI-TEG**, showing higher MSDs. By increasing the content of water up to a 1:3 ratio (300 water molecules), the MSDs increase (from a factor of two up to ten), shifting to bulk-like values. The differences between **NDI-TEG** and **NDI-C6** almost vanish, suggesting that by increasing the water content, the effects of the side chains sizably diminish, and the dynamical behavior of water aggregates starts to resemble that of bulk water at room temperature. The latter observation parallels the results obtained from the structural analyses, where the cases of a 1:3 ratio start to reflect the spatial properties of bulk water at room temperature, regardless of the hydrophilicity or hydrophobicity of the NDI side chains.

After the investigation of the translational dynamics, we examine the time-dependent evolution of the orientational tetrahedral order (q) and of the rotational dynamics of water molecules. To study the changes of q in time, we resort to the time-dependent autocorrelation function C_q,[78] as defined in Eq. (5). The computed C_q for room temperature and supercooled bulk water, 1:1 and 1:3 ratios in **NDI-TEG** and **NDI-C6** are reported in panels (b) and (d) of Fig. 4. As expected, the typical timescales associated to C_q are much faster than the translational dynamics. For bulk water at 300 K, $C_q(t)$ decays to zero (i.e., approaching uncorrelated data) after 15 ps, a timescale shorter than the one characterizing the translational motions (e.g., diffusive or sub-diffusive regimes occur at ≈ 10–10^2 ns). In the supercooled regime (200 K), instead, the local

tetrahedral order is maintained over longer timescales than 300 K, with $C_q(t)$ being equal to 0.5–0.6 for times longer than 10 ps, in very good agreement with literature data.[78] For water confined into NDI crystals, C_q reflects the situation of the supercooled bulk state, preserving the value of the tetrahedral order parameter for longer times than bulk water at room temperature. For the case of 100 water molecules in **NDI-TEG**, C_q seemingly features an initial drop on a shorter timescale than water molecules in **NDI-C6**, resembling the supercooled bulk situation. However, as magnified by the longer timescale behavior of C_q, the differences among the two NDI crystals are not physically and statistically significant. By increasing the content of water up to 300 molecules, there are no relevant variations in C_q, and over the selected timescale, the decays remain comparable with the supercooled water bulk state. Taken together, the analyses of the MSD and C_q further suggest that low-dimensional effects are more important than the hydrophilicity/hydrophobicity characters of the side chains in governing the properties of confined water. Water under confinement in molecular crystals preserves the orientational order for timescales larger than those experienced in the bulk, resembling the situation of a glassy-like state.

We complement the time-dependent structural analyses by studying the reorientational dynamics under confinement (Fig. 5).

Water reorientational dynamics occurs on two distinct timescales: sub-picosecond and picosecond.[79] At the sub-picosecond timescale (<200 fs), water undergoes inertial rotational motion, which is rapidly hindered by hydrogen bonding with neighboring molecules, resulting in librational oscillations. On the picosecond timescale (>2 ps), full molecular reorientation takes place through angular jumps. Although the nature of these latter reorientations is non-local and collective,[81] both phenomena can

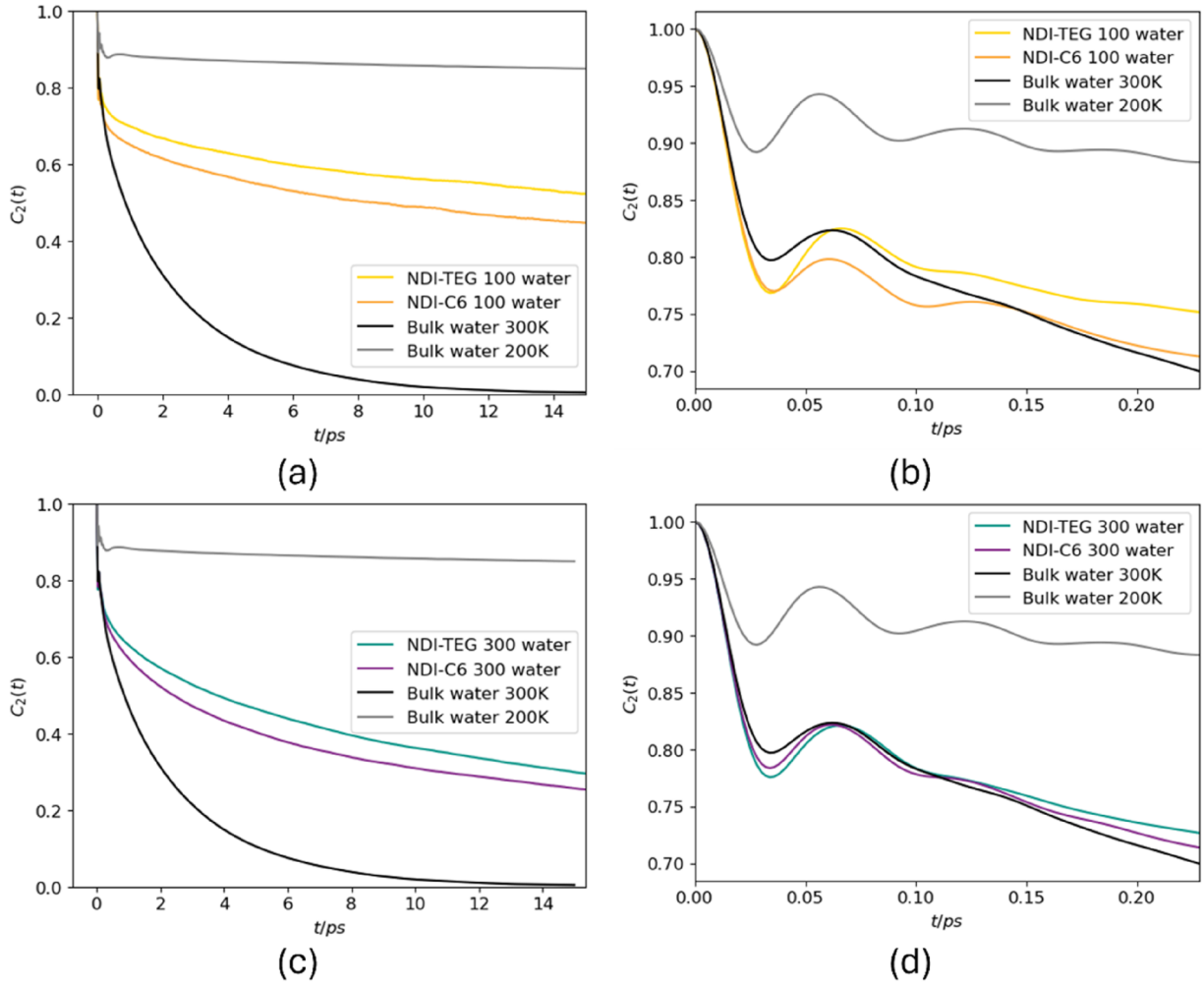

FIG. 5. Reorientational time-correlation function [$C_2(t)$]. $C_2(t)$ of 100 water molecules in **NDI-TEG** and **NDI-C6** for long (15 ps, panel a) and short time scales (0.25 ps, panel b). $C_2(t)$ of 300 water molecules in **NDI-TEG** and **NDI-C6** for long (15 ps, panel c) and short time scales (0.25 ps, panel d). In each panel, bulk water at room temperature is reported in black, while supercooled water (200 K) is shown in gray.

be conveniently captured by the $C_2(t)$ autocorrelation function. Our analyses show that the reorientational dynamics of bulk water at room temperature are consistent with literature data,[82] showing the short timescale librational dynamics and decaying to zero within 15 ps. When supercooled at 200 K, librations are slowed down and partially hindered [Fig. 5(b)]. For confined systems, notably both the 100 and 300 water molecule cases exhibit similar reorientational dynamics as bulk water at room temperature [Figs. 5(b)–5(d)]. This evidence contrasts with the previous analysis on the translational and bond orientational dynamics, where confined water exhibits a behavior closer to the supercooled bulk state. Such an aspect suggests a remarkable observation, namely, that the fast reorientational dynamics (librations) of self-assembled water clusters in molecular crystals are governed by temperature rather than confinement effects. The number of water molecules also affects the absolute value of the correlation function, with the 100 water systems displaying slower reorientational dynamics than the 300 water systems. For the latter, the computed $C_2(t)$ at long time scales (>20 ps) is reported in the supplementary material, showing full decay (<0.1) within 200 ps.

Finally, Fig. 6 shows the autocorrelation functions of the HB network. Depending on the continuous or persistent definition (see the section titled "Methods"), the HB autocorrelation function of bulk water at 300 K decays in ≈1–10 ps. In contrast, supercooled water exhibits a significantly slower decay, indicative of a long-living HB network reflecting the rigid, glassy-like state. Under confinement in NDI crystals, at a low hydration level (1:1 ratio), correlations in the HB network decay more slowly than in bulk water at 300 K for both **NDI-TEG** and **NDI-C6** [Figs. 6(a) and 6(b)]. We attribute this behavior to the small number of confined water molecules, which limits the possible combinations of HB patterns, thus hindering the network dynamics. For higher hydration, e.g., a 1:3 ratio, the

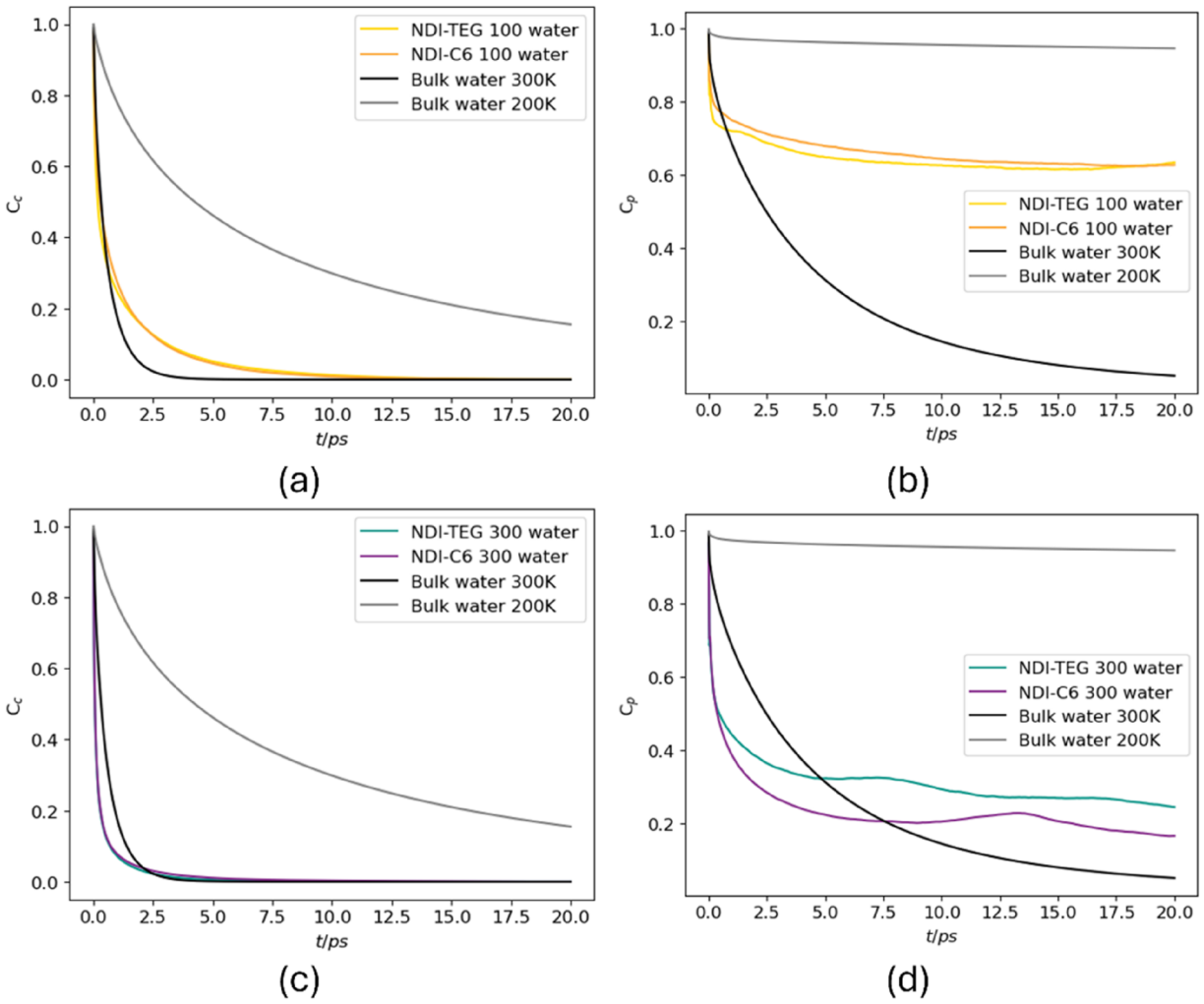

FIG. 6. Continuous (panels a and c) and persistent (panels b and d) HB autocorrelation functions for the case with 100 (panels a and b) and 300 water molecules (panels c and d) in **NDI-TEG** and **NDI-C6** compared with those of room-temperature (solid black line) and supercooled (solid gray line) water.

HB network decays faster than in bulk water at 300 K for both **NDI-TEG** and **NDI-C6** at shorter times, and it decays slightly slower at longer timescales. We argue that the origin of this difference is in the formation of larger water clusters with respect to the 1:1 case (Figs. 2 and 3): at shorter times, small librational motions are sufficient to break the geometric HB criterion, whereas at longer timescales, confinement and the finite size of the water domains in the crystal pockets still limit the complete reorganization of the whole HB network, as also detected for the 100 molecules cases, leading to a residual correlation tail that outlives bulk water.

CONCLUSIONS

We employed classical molecular dynamics simulations to study how water organizes and moves when confined within NDI-based molecular crystals bearing either hydrophilic triethylene glycol (**NDI-TEG**) or hydrophobic n-hexyl (**NDI-C6**) side chains. Structural and dynamical properties were discussed as a function of crystal hydration. By combining bond order descriptors, such as the tetrahedral order parameter (q) and the Lechner–Dellago bond orientational order parameters ($\langle q_4 \rangle$, $\langle q_6 \rangle$), and time-dependent autocorrelation functions, we derived a coherent picture of water properties, elucidating the roles played by the side-chain chemistry (i.e., hydrophobic/hydrophilic), confinement effects, and hydration level.

At low hydration (NDI:water ≈1:1), confinement and side-chain chemistry jointly determine water structural properties. According to the tetrahedral order parameter, water in **NDI-TEG** forms elongated clusters, showing quasi-linear arrangements, while in **NDI-C6**, it does not show any predominant tetrahedral order. The complementary analysis with the Lechner–Dellago parameters shows a higher degree of local bond orientational order for confined water with respect to the bulk and supercooled states. The Lechner–Dellago parameters are therefore not much affected by the nature of side-chains (hydrophobic or hydrophilic), in contrast to the tetrahedral order parameter. Upon increasing hydration (NDI:water ≈1:3), the interplay between confinement and side-chain chemistry becomes dominated by the former. Both the tetrahedral order and the Lechner–Dellago parameters show that confined water structures shift toward bulk liquid, with negligible differences between **NDI-TEG** or **-C6**.

Dynamical properties show a similar trend with increasing crystal hydration. As for the diffusion, the mean-square displacements of confined water at low hydration (NDI:water ≈1:1) and long time-scales (ns) are intermediate between supercooled and liquid-like bulk. Water in **NDI-C6** shows mean-square displacements slightly larger than water in **NDI-TEG**, pointing to the bulk liquid phase. At higher hydration (NDI:water ≈1:3), water displacements increase, getting closer to the liquid-like bulk, with differences between **NDI-TEG** or **NDI-C6** chains vanishing. Such a trend intriguingly suggests that diffusive properties (e.g., ion transport) might become insensitive to the NDI side-chain chemistry, being ultimately governed by the collective properties of the confined water clusters.

Concerning the local orientational order, the autocorrelation function of the tetrahedral order parameter for confined water decays similarly to the supercooled glassy-like state, at timescales of ≈1–20 ps, regardless of the NDI side-chain hydrophilicity or hydrophobicity and the hydration level. This aspect suggests that confinement effects limit the fluctuations of the local orientational order, reducing the possibility for the system to explore the phase-space, unlike the case of bulk liquid.

Reorientational dynamics show a different scenario. At time scales larger than a few (~5) ps and at low hydration (NDI:water ≈1:1), the reorientational dynamics of confined water in NDI crystals are close to those of supercooled water; however, at higher hydration (NDI:water ≈1:3), they become closer to the room temperature case. Water confined in **NDI-TEG** shows slightly faster reorientational dynamics than water in **NDI-C6** at both hydration levels. Notably, fast reorientational dynamics (sub-ps), known as librations, appear to be governed solely by the temperature and not by confinement effects. Changes of the crystal hydration and side-chain functionalization led to the same reorientational dynamics as bulk liquid water.

Finally, the analysis of the hydrogen-bond network autocorrelation functions highlights how finite-size effects and restricted connectivity control network rearrangements. At low hydration (NDI:water ≈1:1), the hydrogen-bond correlation functions decay slower than bulk water due to the limited number of possible hydrogen bond acceptors and donors. At higher hydration (NDI:water ≈1:3), at first, the hydrogen-bond network decays faster than in bulk water and then becomes slower. Under confinement, small oscillations are sufficient to break the geometric criteria of the hydrogen bonds, resulting in fast network modifications, while at longer times, confinement slows down the global network dynamics.

Water confined in NDI-based molecular crystals spans a variety of states between liquid- and glassy-like, resulting in a rich structural and dynamical landscape. Hydration level and confinement are the key variables controlling the properties of water in NDI molecular crystals, while changes in water–crystal interactions (hydrophobicity and hydrophilicity of the side chains) act as a secondary variable for fine-tuning the transport properties.

SUPPLEMENTARY MATERIAL

The supplementary material contains further information concerning the simulation details; the oxygen–oxygen radial distribution functions of hydrated NDI crystals and the q_4/q_6 parameters for each case; the fitting functions for the mean-square displacements and the $C_2(t)$ autocorrelation function; the cluster analyses; and figures reporting the structure of the 1:5 hydration cases.

ACKNOWLEDGMENTS

D.F. acknowledges the National Recovery and Resilience Plan (NRRP), Mission 04 Component 2 Investment 1.5 – NextGenerationEU, Call for Tender No. 3277 dated December 30, 2021, Award No. 0001052 dated June 23, 2022, and the National Project funded by the European Union – Next Generation EU, Project title "Modeling and design of organic conjugated redox materials for energy-saving applications: a bottom-up strategy," code Grant No. MUR 2022WKTH9E – CUP J53D23008810006. D.F., M.S., and F.G. thank Dr. A. Giovine from the Department of Computer Science and Engineering of the University of Bologna for providing full support in the usage of the High-Performance Computing service cluster of

the University of Bologna. D.F. and M.S. thank the ICSC National Research Center for High Performance Computing, Big Data and Quantum Computing for granting computing time on CINECA LEONARDO with the project identifier PICA ID 1700031.

G.A. and G.C. acknowledge support from ICSC – Centro Nazionale di Ricerca in High Performance Computing, Big Data and Quantum Computing, funded by European Union – NextGenerationEU - PNRR, Missione 4 Componente 2 Investimento 1.4. G.C. acknowledges the European Union – NextGeneration EU from the Italian Ministry of Environment and Energy Security POR H2 AdP MMES/ENEA with involvement of CNR and RSE, PNRR - Mission 2, Component 2, Investment 3.5 "Ricerca e sviluppo sull'idrogeno," CUP: B93C22000630006. G.C. acknowledges the European Union (NextGeneration EU), through the MUR-PNRR project SAMOTHRACE (ECS00000022). C.B.N. acknowledges funding from the European Union Horizon Europe under EC Grant Agreement No. 101129638 and from UK Research and Innovation (UKRI) under the UK government's Horizon Europe funding guarantee (Grant No. 10104091).

AUTHOR DECLARATIONS

Conflict of Interest

The authors have no conflicts to disclose.

Author Contributions

F.T.G. and M.S. contributed equally to this work.

Filippo Tommaso Garattoni: Conceptualization (equal); Data curation (equal); Formal analysis (equal); Investigation (equal); Methodology (equal). **Marco Severi**: Conceptualization (equal); Data curation (equal); Formal analysis (equal); Investigation (equal); Methodology (equal); Writing – original draft (equal); Writing – review & editing (equal). **Gabriele Amante**: Data curation (equal); Formal analysis (equal); Writing – original draft (equal); Writing – review & editing (equal). **Christian B. Nielsen**: Conceptualization (supporting); Writing – original draft (supporting); Writing – review & editing (supporting). **Giuseppe Cassone**: Data curation (equal); Formal analysis (equal); Funding acquisition (supporting); Methodology (supporting); Writing – original draft (equal); Writing – review & editing (equal). **Daniele Fazzi**: Conceptualization (lead); Data curation (supporting); Formal analysis (equal); Funding acquisition (lead); Investigation (equal); Methodology (equal); Project administration (lead); Supervision (lead); Writing – original draft (lead); Writing – review & editing (lead).

DATA AVAILABILITY

The data that support the findings of this study are available within the article and its supplementary material.

REFERENCES

[1] C. Goy, G. Kimmel, Y. Jiang, and C. Valeriani, "Advances in unveiling water's molecular mysteries," J. Chem. Phys. **163**(11), 110401 (2025).
[2] F. Leoni, C. Calero, and G. Franzese, "Nanoconfined fluids: Uniqueness of water compared to other liquids," ACS Nano **15**(12), 19864–19876 (2021).
[3] A. Omranpour, P. Montero De Hijes, J. Behler, and C. Dellago, "Perspective: Atomistic simulations of water and aqueous systems with machine learning potentials," J. Chem. Phys. **160**(17), 170901 (2024).
[4] M. I. Oh, M. Gupta, C. I. Oh, and D. F. Weaver, "Understanding the effect of nanoconfinement on the structure of water hydrogen bond networks," Phys. Chem. Chem. Phys. **21**(47), 26237–26250 (2019).
[5] R. Musat, J. P. Renault, M. Candelaresi, D. J. Palmer, S. Le Caër, R. Righini, and S. Pommeret, "Finite size effects on hydrogen bonds in confined water," Angew. Chem., Int. Ed. **47**(42), 8033–8035 (2008).
[6] C. Calero and G. Franzese, "Water under extreme confinement in graphene: Oscillatory dynamics, structure, and hydration pressure explained as a function of the confinement width," J. Mol. Liq. **317**, 114027 (2020).
[7] S. Dasgupta, S. Saha, and F. Paesani, "Sub-nanometer confinement suppresses autoionization of water," J. Am. Chem. Soc. **147**(29), 25167–25173 (2025).
[8] S. Dasgupta, S. Saha, and F. Paesani, "Reactivity of nanoconfined water is modulated by the properties of confining materials," J. Phys. Chem. Lett. **16**(46), 11996–12004 (2025).
[9] J. Lucid, S. Meloni, D. MacKernan, E. Spohr, and G. Ciccotti, "Probing the structures of hydrated nafion in different morphologies using temperature-accelerated molecular dynamics simulations," J. Phys. Chem. C **117**(2), 774–782 (2013).
[10] S. Bonella, D. Raimondo, E. Milanetti, A. Tramontano, and G. Ciccotti, "Mapping the hydropathy of amino acids based on their local solvation structure," J. Phys. Chem. B **118**(24), 6604–6613 (2014).
[11] R. Horstmann, L. Hecht, S. Kloth, and M. Vogel, "Structural and dynamical properties of liquids in confinements: A review of molecular dynamics simulation studies," Langmuir **38**(21), 6506–6522 (2022).
[12] I. N. Tsimpanogiannis, O. A. Moultos, L. F. M. Franco, M. B. d. M. Spera, M. Erdős, and I. G. Economou, "Self-diffusion coefficient of bulk and confined water: A critical review of classical molecular simulation studies," Mol. Simul. **45**(4–5), 425–453 (2019).
[13] L. Fumagalli, A. Esfandiar, R. Fabregas, S. Hu, P. Ares, A. Janardanan, Q. Yang, B. Radha, T. Taniguchi, K. Watanabe, G. Gomila, K. S. Novoselov, and A. K. Geim, "Anomalously low dielectric constant of confined water," Science **360**(6395), 1339–1342 (2018).
[14] D. Borgis, D. Laage, L. Belloni, and G. Jeanmairet, "Dielectric response of confined water films from a classical density functional theory perspective," Chem. Sci. **14**(40), 11141–11150 (2023).
[15] S. De Luca, S. K. Kannam, B. D. Todd, F. Frascoli, J. S. Hansen, and P. J. Daivis, "Effects of confinement on the dielectric response of water extends up to mesoscale dimensions," Langmuir **32**(19), 4765–4773 (2016).
[16] R. Wang, M. Souilamas, A. Esfandiar, R. Fabregas, S. Benaglia, H. Nevison-Andrews, Q. Yang, J. Normansell, P. Ares, G. Ferrari, A. Principi, A. K. Geim, and L. Fumagalli, "In-plane dielectric constant and conductivity of confined water," Nature **646**(8085), 606–610 (2025).
[17] P. Li, X. Yang, F. Chen, D. Wang, D. Hao, Z. Xu, M. Qiu, S. He, F. Xia, and Y. Tian, "Confined water dominates ion/molecule transport in hydrogel nanochannels," Nano Lett. **24**(3), 897–904 (2024).
[18] S. Liao, Y. Liu, L. Li, L. Ding, Y. Wei, and H. Wang, "Theoretical framework for confined ion transport in two-dimensional nanochannels," Nat. Commun. **16**(1), 6675 (2025).
[19] Y. Ishii, N. Matubayasi, G. Watanabe, T. Kato, and H. Washizu, "Molecular insights on confined water in the nanochannels of self-assembled ionic liquid crystal," Sci. Adv. **7**(31), eabf0669 (2021).
[20] P. Hirunsit and P. B. Balbuena, "Effects of confinement on small water clusters structure and proton transport," J. Phys. Chem. A **111**(42), 10722–10731 (2007).
[21] T. Wang, H. Iriawan, J. Peng, R. R. Rao, B. Huang, D. Zheng, D. Menga, A. Aggarwal, S. Yuan, J. Eom, Y. Zhang, K. McCormack, Y. Román-Leshkov, J. Grossman, and Y. Shao-Horn, "Confined water for catalysis: Thermodynamic properties and reaction kinetics," Chem. Rev. **125**(3), 1420–1467 (2025).
[22] Y. Sun, C. Zhan, P. R. C. Kent, M. Naguib, Y. Gogotsi, and D.-e. Jiang, "Proton redox and transport in MXene-confined water," ACS Appl. Mater. Interfaces **12**(1), 763–770 (2020).
[23] S. Melnik, A. Ryzhov, A. Kiselev, A. Radenovic, T. Weil, K. J. Stevenson, and V. G. Artemov, "Confinement-controlled water engenders unusually high electrochemical capacitance," J. Phys. Chem. Lett. **14**(29), 6572–6576 (2023).

[24]S. Capponi, S. H. White, D. J. Tobias, and M. Heyden, "Structural relaxation processes and collective dynamics of water in biomolecular environments," J. Phys. Chem. B **123**(2), 480–486 (2019).
[25]S. Capponi, M. Heyden, A.-N. Bondar, D. J. Tobias, and S. H. White, "Anomalous behavior of water inside the SecY translocon," Proc. Natl. Acad. Sci. U. S. A. **112**(29), 9016–9021 (2015).
[26]L. Tavagnacco, M. Zanatta, E. Buratti, M. Bertoldo, E. Chiessi, M. Appel, F. Natali, A. Orecchini, and E. Zaccarelli, "Water slowing down drives the occurrence of the low temperature dynamical transition in microgels," Chem. Sci. **15**(24), 9249–9257 (2024).
[27]L. Tavagnacco, E. Chiessi, M. Zanatta, A. Orecchini, and E. Zaccarelli, "Water–Polymer coupling induces a dynamical transition in microgels," J. Phys. Chem. Lett. **10**(4), 870–876 (2019).
[28]K. E. Karim, M. Barisik, C. Bakli, and B. Kim, "Estimating water transport in carbon nanotubes: A critical review and inclusion of scale effects," Phys. Chem. Chem. Phys. **26**(28), 19069–19082 (2024).
[29]A. Srivastava, S. Abedrabbo, J. Hassan, and D. Homouz, "Dynamics of confined water inside carbon nanotubes based on studying tetrahedral order parameters," Sci. Rep. **14**(1), 15480 (2024).
[30]C.-W. Wang, Y.-W. Kuo, J.-R. Zeng, P.-H. Tang, and T.-M. Wu, "Confinement effects on reorientation dynamics of water confined within graphite nanoslits," J. Phys. Chem. B **128**(39), 9525–9535 (2024).
[31]Q. Li, J. Song, F. Besenbacher, and M. Dong, "Two-dimensional material confined water," Acc. Chem. Res. **48**(1), 119–127 (2015).
[32]S. Merchiori, A. Le Donne, J. D. Littlefair, A. R. Lowe, J.-J. Yu, X.-D. Wu, M. Li, D. Li, M. Geppert-Rybczyńska, L. Scheller, B. A. Trump, A. A. Yakovenko, P. Zajdel, M. Chorążewski, Y. Grosu, and S. Meloni, "Mild-temperature supercritical water confined in hydrophobic metal–organic frameworks," J. Am. Chem. Soc. **146**(19), 13236–13246 (2024).
[33]A. J. Rieth, K. M. Hunter, M. Dincă, and F. Paesani, "Hydrogen bonding structure of confined water templated by a metal-organic framework with open metal sites," Nat. Commun. **10**(1), 4771 (2019).
[34]L. Tavagnacco, E. Chiessi, L. Severini, S. Franco, E. Buratti, A. Capocefalo, F. Brasili, A. Mosca Conte, M. Missori, R. Angelini, S. Sennato, C. Mazzuca, and E. Zaccarelli, "Molecular origin of the two-step mechanism of gellan aggregation," Sci. Adv. **9**(10), eadg4392 (2023).
[35]N. A. Kukhta, A. Marks, and C. K. Luscombe, "Molecular design strategies toward improvement of charge injection and ionic conduction in organic mixed ionic–electronic conductors for organic electrochemical transistors," Chem. Rev. **122**(4), 4325–4355 (2022).
[36]P. Gkoupidenis, Y. Zhang, H. Kleemann, H. Ling, F. Santoro, S. Fabiano, A. Salleo, and Y. van de Burgt, "Organic mixed conductors for bioinspired electronics," Nat. Rev. Mater. **9**(2), 134–149 (2023).
[37]M. Al Kobaisi, S. V. Bhosale, K. Latham, A. M. Raynor, and S. V. Bhosale, "Functional naphthalene diimides: Synthesis, properties, and applications," Chem. Rev. **116**(19), 11685–11796 (2016).
[38]S. V. Bhosale, M. Al Kobaisi, R. W. Jadhav, P. P. Morajkar, L. A. Jones, and S. George, "Naphthalene diimides: Perspectives and promise," Chem. Soc. Rev. **50**(17), 9845–9998 (2021).
[39]"Conducting polymers forward," Nat. Mater. **19**(9), 921 (2020).
[40]C. B. Nielsen, A. Giovannitti, D.-T. Sbircea, E. Bandiello, M. R. Niazi, D. A. Hanifi, M. Sessolo, A. Amassian, G. G. Malliaras, J. Rivnay, and I. McCulloch, "Molecular design of semiconducting polymers for high-performance organic electrochemical transistors," J. Am. Chem. Soc. **138**(32), 10252–10259 (2016).
[41]B. D. Paulsen, K. Tybrandt, E. Stavrinidou, and J. Rivnay, "Organic mixed ionic–electronic conductors," Nat. Mater. **19**(1), 13–26 (2020).
[42]N. Siemons, D. Pearce, C. Cendra, H. Yu, S. M. Tuladhar, R. K. Hallani, R. Sheelamanthula, G. S. LeCroy, L. Siemons, A. J. P. White, I. McCulloch, A. Salleo, J. M. Frost, A. Giovannitti, and J. Nelson, "Impact of side-chain hydrophilicity on packing, swelling, and ion interactions in oxy-bithiophene semiconductors," Adv. Mater. **34**(39), 2204258 (2022).
[43]D. Moia, A. Giovannitti, A. A. Szumska, I. P. Maria, E. Rezasoltani, M. Sachs, M. Schnurr, P. R. F. Barnes, I. McCulloch, and J. Nelson, "Design and evaluation of conjugated polymers with polar side chains as electrode materials for electrochemical energy storage in aqueous electrolytes," Energy Environ. Sci. **12**(4), 1349–1357 (2019).
[44]A. Giovannitti, I. P. Maria, D. Hanifi, M. J. Donahue, D. Bryant, K. J. Barth, B. E. Makdah, A. Savva, D. Moia, M. Zetek, P. R. F. Barnes, O. G. Reid, S. Inal, G. Rumbles, G. G. Malliaras, J. Nelson, J. Rivnay, and I. McCulloch, "The role of the side chain on the performance of N-type conjugated polymers in aqueous electrolytes," Chem. Mater. **30**(9), 2945–2953 (2018).
[45]N. Siemons, D. Pearce, H. Yu, S. M. Tuladhar, G. S. LeCroy, R. Sheelamanthula, R. K. Hallani, A. Salleo, I. McCulloch, A. Giovannitti, J. M. Frost, and J. Nelson, "Controlling swelling in mixed transport polymers through alkyl side-chain physical cross-linking," Proc. Natl. Acad. Sci. U. S. A. **120**(35), e2306272120 (2023).
[46]S. Moro, N. Siemons, O. Drury, D. A. Warr, T. A. Moriarty, L. M. A. Perdigão, D. Pearce, M. Moser, R. K. Hallani, J. Parker, I. McCulloch, J. M. Frost, J. Nelson, and G. Costantini, "The effect of glycol side chains on the assembly and microstructure of conjugated polymers," ACS Nano **16**(12), 21303–21314 (2022).
[47]Y. Tsarfati, K. C. Bustillo, B. H. Savitzky, L. Balhorn, T. J. Quill, A. Marks, J. Donohue, S. E. Zeltmann, C. J. Takacs, A. Giovannitti, I. McCulloch, C. Ophus, A. M. Minor, and A. Salleo, "The hierarchical structure of organic mixed ionic–electronic conductors and its evolution in water," Nat. Mater. **24**(1), 101–108 (2025).
[48]N. Siemons, A. De La Fuente Durán, A. C. Shad, M. Iyer, F.-Y. Chen, A. Marks, W. Chueh, and A. Salleo, "The importance of organic mixed ionic-electronic conductor (OMIEC)–water interactions: A perspective," J. Am. Chem. Soc. **147**(45), 41193–41203 (2025).
[49]H. Yu, A. Marks, S. M. Tuladhar, N. Siemons, I. Anderson, S. Bidinger, S. T. Keene, T. J. Quill, R. Wu, O. Gough, G. Wu, F. Eisner, A. Salleo, J. Rivnay, G. G. Malliaras, P. R. F. Barnes, I. McCulloch, and J. Nelson, "The influence of alkyl spacers and molecular weight on the charge transport and storage properties of oxy-bithiophene-based conjugated polymers," Angew. Chem. **137**(6), e202417897 (2025).
[50]Z. Wang, G. Sun, N. H. C. Lewis, M. Mandal, A. Sharma, M. Kim, J. M. Montes de Oca, K. Wang, A. Taggart, A. B. Martinson, P. A. Kohl, A. Tokmakoff, S. N. Patel, P. F. Nealey, and J. J. de Pablo, "Water-mediated ion transport in an anion exchange membrane," Nat. Commun. **16**(1), 1099 (2025).
[51]M. Severi, S. Yu, I. Abrahams, C. B. Nielsen, and D. Fazzi, "Disclosing the molecular structure and dynamics of naphthalene diimide based organic semiconductors in the solid state," J. Mater. Chem. C **14**(1), 385–396 (2026).
[52]D. Shukla, S. F. Nelson, D. C. Freeman, M. Rajeswaran, W. G. Ahearn, D. M. Meyer, and J. T. Carey, "Thin-film morphology control in naphthalene-diimide-based semiconductors: High mobility n-type semiconductor for organic thin-film transistors," Chem. Mater. **20**(24), 7486–7491 (2008).
[53]S. Milita, F. Liscio, L. Cowen, M. Cavallini, B. A. Drain, T. Degousée, S. Luong, O. Fenwick, A. Guagliardi, B. C. Schroeder, and N. Masciocchi, "Polymorphism in N,N′-dialkyl-naphthalene diimides," J. Mater. Chem. C **8**(9), 3097–3112 (2020).
[54]I. d. O. Martins, F. Marin, E. Modena, and L. Maini, "On the crystal forms of NDI-C6: Annealing and deposition procedures to access elusive polymorphs," Faraday Discuss. **235**, 490–507 (2022).
[55]S. Cerveny, F. Mallamace, J. Swenson, M. Vogel, and L. Xu, "Confined water as model of supercooled water," Chem. Rev. **116**(13), 7608–7625 (2016).
[56]P. G. Debenedetti and F. H. Stillinger, "Supercooled liquids and the glass transition," Nature **410**(6825), 259–267 (2001).
[57]J. R. Errington and P. G. Debenedetti, "Relationship between structural order and the anomalies of liquid water," Nature **409**(6818), 318–321 (2001).
[58]W. Lechner and C. Dellago, "Accurate determination of crystal structures based on averaged local bond order parameters," J. Chem. Phys. **129**(11), 114707 (2008).
[59]A. P. Thompson, H. M. Aktulga, R. Berger, D. S. Bolintineanu, W. M. Brown, P. S. Crozier, P. J. in't Veld, A. Kohlmeyer, S. G. Moore, T. D. Nguyen, R. Shan, M. J. Stevens, J. Tranchida, C. Trott, and S. J. Plimpton, "LAMMPS—A flexible simulation tool for particle-based materials modeling at the atomic, meso, and continuum scales," Comput. Phys. Commun. **271**, 108171 (2022).
[60]W. L. Jorgensen, M. M. Ghahremanpour, A. Saar, and J. Tirado-Rives, "OPLS/2020 force field for unsaturated hydrocarbons, alcohols, and ethers," J. Phys. Chem. B **128**(1), 250–262 (2024).
[61]A. Tkatchenko and M. Scheffler, "Accurate molecular Van Der Waals interactions from ground-state electron density and free-atom reference data," Phys. Rev. Lett. **102**(7), 073005 (2009).

[62]K.-H. Lin, L. Paterson, F. May, and D. Andrienko, "Glass transition temperature prediction of disordered molecular solids," npj Comput. Mater. **7**(1), 179 (2021).
[63]D. J. Cole, J. Z. Vilseck, J. Tirado-Rives, M. C. Payne, and W. L. Jorgensen, "Biomolecular force field parameterization via atoms-in-molecule electron density partitioning," J. Chem. Theory Comput. **12**(5), 2312–2323 (2016).
[64]T. A. Manz and N. G. Limas, "Introducing DDEC6 atomic population analysis: Part 1. Charge partitioning theory and methodology," RSC Adv. **6**(53), 47771–47801 (2016).
[65]N. G. Limas and T. A. Manz, "Introducing DDEC6 atomic population analysis: Part 2. Computed results for a wide range of periodic and nonperiodic materials," RSC Adv. **6**(51), 45727–45747 (2016).
[66]T. A. Manz, "Introducing DDEC6 atomic population analysis: Part 3. Comprehensive method to compute bond orders," RSC Adv. **7**(72), 45552–45581 (2017).
[67]N. G. Limas and T. A. Manz, "Introducing DDEC6 atomic population analysis: Part 4. Efficient parallel computation of net atomic charges, atomic spin moments, bond orders, and more," RSC Adv. **8**(5), 2678–2707 (2018).
[68]S. Izadi and A. V. Onufriev, "Accuracy limit of rigid 3-point water models," J. Chem. Phys. **145**(7), 074501 (2016).
[69]S. P. Kadaoluwa Pathirannahalage, N. Meftahi, A. Elbourne, A. C. G. Weiss, C. F. McConville, A. Padua, D. A. Winkler, M. Costa Gomes, T. L. Greaves, T. C. Le, Q. A. Besford, and A. J. Christofferson, "Systematic comparison of the structural and dynamic properties of commonly used water models for molecular dynamics simulations," J. Chem. Inf. Model. **61**(9), 4521–4536 (2021).
[70]E. Duboué-Dijon and D. Laage, "Characterization of the local structure in liquid water by various order parameters," J. Phys. Chem. B **119**(26), 8406–8418 (2015).
[71]H. Tanaka, H. Tong, R. Shi, and J. Russo, "Revealing key structural features hidden in liquids and glasses," Nat. Rev. Phys. **1**(5), 333–348 (2019).
[72]Z. Yan, S. V. Buldyrev, P. Kumar, N. Giovambattista, P. G. Debenedetti, and H. E. Stanley, "Structure of the first- and second-neighbor shells of simulated water: Quantitative relation to translational and orientational order," Phys. Rev. E **76**(5), 051201 (2007).
[73]P. J. Steinhardt *et al.*, "Bond-orientational order in liquids and glasses," Phys. Rev. B **28**(2), 784–805 (1983).
[74]A. J. Mukhtyar and F. A. Escobedo, "Developing local order parameters for order–disorder transitions from particles to block copolymers: Methodological framework," Macromolecules **51**(23), 9769–9780 (2018).
[75]S. Jungblut and C. Dellago, "Crystallization of a binary Lennard-Jones mixture," J. Chem. Phys. **134**(10), 104501 (2011).
[76]M. Brehm and B. Kirchner, "TRAVIS—A free analyzer and visualizer for Monte Carlo and molecular dynamics trajectories," J. Chem. Inf. Model. **51**(8), 2007–2023 (2011).
[77]M. Brehm, M. Thomas, S. Gehrke, and B. Kirchner, "TRAVIS—A free analyzer for trajectories from molecular simulation," J. Chem. Phys. **152**(16), 164105 (2020).
[78]P. Kumar, S. V. Buldyrev, and H. E. Stanley, "A tetrahedral entropy for water," Proc. Natl. Acad. Sci. U. S. A. **106**(52), 22130–22134 (2009).
[79]D. Laage, G. Stirnemann, F. Sterpone, R. Rey, and J. T. Hynes, "Reorientation and allied dynamics in water and aqueous solutions," Annu. Rev. Phys. Chem. **62**, 395–416 (2011).
[80]A. Luzar and D. Chandler, "Hydrogen-bond kinetics in liquid water," Nature **379**(6560), 55–57 (1996).
[81]A. Offei-Danso, U. N. Morzan, A. Rodriguez, A. Hassanali, and A. Jelic, "The collective burst mechanism of angular jumps in liquid water," Nat. Commun. **14**(1), 1345 (2023).
[82]D. Laage and J. T. Hynes, "A molecular jump mechanism of water reorientation," Science **311**(5762), 832–835 (2006).